ROYAL SOCIETY OF CHEMISTRY

EDGE ARTICLE

Check for updates

Site-specific doping of silver atoms into a Au$_{25}$ nanocluster as directed by ligand binding preferences†

Wan-Qi Shi,[a] Zong-Jie Guan,[a] Jiao-Jiao Li,[a] Xu-Shuang Han[a] and Quan-Ming Wang (ID) *[ab]

For the first time site-specific doping of silver into a spherical Au$_{25}$ nanocluster has been achieved in [Au$_{19}$Ag$_6$(MeOPhS)$_{17}$(PPh$_3$)$_6$] (BF$_4$)$_2$ (**Au$_{19}$Ag$_6$**) through a dual-ligand coordination strategy. Single crystal X-ray structural analysis shows that the cluster has a distorted centered icosahedral Au@Au$_6$Ag$_6$ core of D_3 symmetry, in contrast to the I_h Au@Au$_{12}$ kernel in the well-known [Au$_{25}$(SR)$_{18}$]$^-$ (R = CH$_2$CH$_2$Ph). An interesting feature is the coexistence of [Au$_2$(SPhOMe)$_3$] dimeric staples and [P–Au–SPhOMe] semi-staples in the title cluster, due to the incorporation of PPh$_3$. The observation of only one double-charged peak in ESI-TOF-MS confirms the ordered doping of silver atoms. **Au$_{19}$Ag$_6$** is a 6e system showing a distinct absorption spectrum from [Au$_{25}$(SR)$_{18}$]$^-$, that is, the HOMO–LUMO transition of **Au$_{19}$Ag$_6$** is optically forbidden due to the P character of the superatomic frontier orbitals.

1. Introduction

Atomically precise bimetallic nanoclusters have attracted intense attention owing to their structural diversities and potential applications.[1–9] Gold–silver nanoclusters exhibit different catalytic, electrochemical and optical properties compared to their homometallic analogues, and the properties vary with the degree of doping.[10–15] For example, Au$_{57}$Ag$_{53}$(C≡CPh)$_{40}$Br$_{12}$ has a distinctly different optical absorption profile from [Au$_{80}$Ag$_{30}$(C≡CPh)$_{42}$Cl$_9$]Cl, owing to their different metal arrangements and Au/Ag ratios.[16,17] [Au$_{25-x}$Ag$_x$(SR)$_5$(PPh$_3$)$_{10}$Cl$_2$]$^{2+}$ ($x \leq 13$) has a 200-fold increase in luminescence quantum yield after doping the 13th Ag atom.[18] These results indicate that the doping number and position of silver atoms should be considered in studying the structure–property relationships of alloy clusters.[10,19,20]

The thiolated gold nanocluster [Au$_{25}$(SR)$_{18}$]$^-$ (R = CH$_2$CH$_2$-Ph)[21,22] has been extensively used as a parental cluster for heterometal doping, because of its easy preparation and high stability.[23] In 2010, Au$_{25-x}$Ag$_x$(SR)$_{18}$ nanoclusters with x up to 11 were synthesized by Negishi *et al.*,[24] and similar doping reactions were also reported by Murray *et al.*[25] The structure of Au$_{25-x}$Ag$_x$(SR)$_{18}$ was determined by Dass *et al.*,[26] which revealed

a disordered arrangement of the icosahedral shell in Au$_1$@Au$_{5.3}$Ag$_{6.7}$@6×Au$_2$(SR)$_3$. Later, different degrees of doping were achieved, including heavy-doped Au$_{25-x}$Ag$_x$(SR)$_{18}$ (x = 19.4, 20.45) by Jin *et al.*[27,28] Although various degrees of doping can be roughly controlled by regulating the Au/Ag ratios in synthesis procedures, all these clusters are mixtures containing different numbers of heteroatoms as revealed by mass spectrometry.[12,29–32] To establish a direct structure–property correlation, precise doping of heteroatoms in an ordered manner is highly demanded. Such a site-specific doping remains a big challenge, especially for Au–Ag alloy nanoclusters. The difficulty in obtaining non-disordered gold-silver alloy clusters lies mainly in the similarity in the atomic radius and electronic structures of Ag and Au.[23] The substitution of silver atoms at equivalent sites of gold often occurs during heteroatom doping, leading to a distribution of Ag heteroatoms in a gold cluster. For example, the highly symmetric geometry of [Au$_{25}$(SR)$_{18}$]$^-$ makes the surface gold atoms hard to be distinguished, which increases the difficulty of site-specific doping.[33]

It is well known that surface organic ligands are critical in the formation of atomically precise metal nanoclusters.[6,34–40] It has been found that the electronic nature, coordination preference, and bulkiness of ligands can have significant effects on the structures and properties of the clusters.[41–45] In order to achieve site-specific doping of silver into a gold nanocluster, we develop a strategy to control the atomic arrangement through the combination of ligands with different ligating preferences. The use of thiolate and phosphine ligands resulted in the formation of a novel ordered **Au$_{19}$Ag$_6$** core different from those with disordered Au$_{25-x}$Ag$_x$ cores. It is remarkable that the silver

[a]Department of Chemistry, Tsinghua University, Beijing, 100084, PR China. E-mail: qmwang@tsinghua.edu.cn

[b]Department of Chemistry, College of Chemistry and Chemical Engineering, Xiamen University, Xiamen, 361005, PR China

† Electronic supplementary information (ESI) available. CCDC 2131886. For ESI and crystallographic data in CIF or other electronic format see DOI: 10.1039/d2sc00012a

atoms are located at specific positions in the M_{13} kernel due to the different affinities of surface motifs.

Herein, we report the synthesis and structural determination of such an alloy $(Au/Ag)_{25}$ cluster with ordered doping with the formula $[Au_{19}Ag_6(MeOPhS)_{17}(PPh_3)_6](BF_4)_2$ (denoted as **$Au_{19}Ag_6$**). The composition and structure have been determined by electrospray ionization time-of-flight mass spectrometry and single-crystal X-ray structural analysis. An interesting feature is the coexistence of $[Au_2(SPhOMe)_3]$ dimeric staples and $[P–Au–SPhOMe]$ semi-staples in this cluster, due to the incorporation of PPh_3, which dictates the specific sites for dopant silver atoms. In addition, we have also studied the optical properties and electronic structure of this 6e system, which are quite different from $Au_{25-x}Ag_x(SR)_{18}$ clusters.

2. Experimental

2.1 Materials

Triphenylphosphine (Ph_3P, 99.5%), 2,2′-dipyridylamine (Hdpa), 4-methoxythiophenol and silver tetrafluoroborate ($AgBF_4$, 99.0%) were purchased from J&K; sodium borohydride ($NaBH_4$, 98%) and other reagents employed were purchased from Sinopharm Chemical Reagent Co. Ltd (Shanghai, China). All the reagents were used as received without further purification. Me_2SAuCl and Ph_3PAuCl were prepared according to literature methods.[46,47]

2.2 Synthesis of MeOPhSAu

To 60.0 ml acetone containing Me_2SAuCl (589.2 mg, 2.0 mmol), MeOPhSH (336.4 mg, 2.4 mmol) and triethylamine (242.8 mg, 2.4 mmol) were added under vigorous stirring, and the mixture was stirred for 15 minutes in the dark. A large amount of white precipitate was formed. The resulting solution was rotary evaporated to dryness to give a white solid, which was washed with water, ethanol, and ether to give MeOPhSAu.

2.3 Synthesis of MeOPhSAg

10 ml ethanol solution of MeOPhSH (350.5 mg, 2.5 mmol) was dropwise added into 100 ml aqueous solution of $AgNO_3$ (425.0 mg, 2.5 mmol), followed by the addition of triethylamine (242.8 mg, 2.4 mmol), and the solution turned black. In an ice-water bath, the mixture was stirred for 15 minutes in the dark. After suction filtration, the obtained solid was washed with water, ethanol, and ether to give MeOPhSAg.

2.4 Synthesis of $Au_{19}Ag_6$

To 4.0 ml CH_2Cl_2 containing Ph_3PAuCl (24.7 mg, 0.05 mmol), 0.1 ml of methanol solution of $AgBF_4$ (8.8 mg, 0.045 mmol) was added under vigorous stirring. After stirring for 15 minutes in the dark, the mixture was centrifuged and filtered to remove the AgCl precipitate. Hdpa (4.2 mg, 0.025 mmol) was added to the filtrate, the solution turned pale yellow, and the solution was stirred for 1 hour in the dark. Subsequently, MeOPhSAu (16.8 mg, 0.05 mmol) was added, and freshly prepared $NaBH_4$ (0.7 mg in 1 ml ethanol) was added dropwise under stirring. The color of the solution changed from yellow to orange and then to

dark brown. After stirring for 4 hours in the dark, MeOPhSAg (12.4 mg, 0.05 mmol) was added under stirring, and the color of the solution changed from dark brown to brown-black. The reaction solution was stirred for 12 hours at room temperature in the absence of light. After the reaction, the solvent was rotary evaporated to give a dark brown solid. The solid was dissolved in 2.0 ml of dichloromethane and centrifuged at 10 000 rpm for 3 minutes. The dark brown solution was collected, to which *n*-hexane was added for diffusion at 4 °C. After two weeks, black crystals were obtained (10.5 mg, yield 18% based on Au).

2.5 Characterization

UV-Vis-NIR absorption spectra were recorded on a Cary 5000. The mass spectrum was recorded on an ABI4800plus ESI-TOF-MS and a Waters Q-TOF mass spectrometer. Crystals of **$Au_{19}Ag_6$** were dissolved in CH_2Cl_2 for ESI-MS measurement. X-ray photoelectron spectroscopy was performed using a Thermo ESCALAB Xi+ instrument. Intensity data of **$Au_{19}Ag_6$** were collected on an Oxford Gemini S Ultra system (Cu Kα). Absorption corrections were applied by using the program CrysAlis (multi-scan). The structure was solved by direct methods, and non-hydrogen atoms except solvent molecules and counteranions were refined anisotropically by least-squares on F^2 using the SHELXTL program. The diffuse electron densities resulting from the residual solvent molecules were removed from the data set using the Olex2 solvent mask.

2.6 Computational details

Density functional theory (DFT) calculations were performed with the quantum chemistry program Gaussian 16.[48] In the calculations, **$Au_{19}Ag_6$** was mimicked by a model system of $[Au_{19}Ag_6(PH_3)_6(SH)_{17}]^{2+}$. The 6-31G(d) basis set was used for H, S, P, and LANL2DZ, for Au and Ag.[49,50] Geometry optimizations were performed with the B3LYP functional, and time-dependent DFT calculations of the UV-Vis absorption spectrum were performed with the PBE0 functional.[51] One hundred singlet states (nstates = 100, singlet) are chosen in the calculations of the UV-Vis absorption spectra. All the transitions together with their oscillator strengths were then convoluted with a Gaussian line shape of 0.15 eV broadening to make the whole optical-absorption spectrum. The molecular orbitals were visualized *via* the Multiwfn software and the VMD package.[52,53]

3. Results and discussion

The synthesis of **$Au_{19}Ag_6$** involves the reduction of the gold precursor followed by the addition of silver thiolate. It is very important to remove chloride from Ph_3PAuCl, otherwise the known $[(p\text{-}Tol_3P)_{10}Au_{13}Ag_{12}Cl_8]$ (PF_6) with a biicosahedral core is obtained as reported previously.[54] The halide-free strategy has been proved successful in synthesizing new phosphine/thiolate co-protected metal nanoclusters such as $[Au_{55}(p\text{-}MBT)_{24}(Ph_3\text{-}P)_6](SbF_6)_3$ (*p*-MBT = 4-methylbenzenethiolate).[55]

The composition of **$Au_{19}Ag_6$** was determined by electrospray ionization time-of-flight mass spectrometry (ESI-TOF-MS) in positive-ion mode. As shown in Fig. 1, there is only one doubly
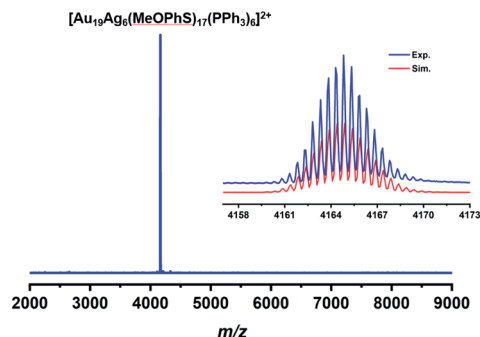
Fig. 1 ESI-TOF-MS spectrum of **Au$_{19}$Ag$_6$** in CH$_2$Cl$_2$. Inset: comparison of the experimental (blue) and simulated (red) isotope distribution patterns.

charged peak observed at *m/z* 4164.83, which corresponds to the molecular ion [Au$_{19}$Ag$_6$(MeOPhS)$_{17}$(PPh$_3$)$_6$]$^{2+}$. The isotopic distribution pattern is in perfect agreement with the simulated one (Fig. 1, inset). No other doping products with different numbers of silver atoms were observed. The small doubly charged peak at *m/z* 4332.8 corresponds to [Au$_{20}$Ag$_6$(-MeOPhS)$_{18}$(PPh$_3$)$_6$]$^{2+}$, due to the incorporation of MeOPhSAu into [Au$_{19}$Ag$_6$(MeOPhS)$_{17}$(PPh$_3$)$_6$]$^{2+}$.

The gold 4f$_{7/2}$ binding energy of **Au$_{19}$Ag$_6$** is 84.2 eV that is in between that of Au(0) (84.0 eV) and Au(1) (84.9 eV), confirming that gold atoms in **Ag$_{19}$Ag$_6$** exist in mixed oxidation states of Au(0) and Au(I). The Ag 3d$_{5/2}$ binding energy is 367.6 eV that is significantly lower than that of metallic silver (368.27 eV), indicating that Ag atoms in the cluster are positively charged.[13]

The structure of **Au$_{19}$Ag$_6$** was determined by X-ray single-crystal diffraction.[56] As shown in Fig. 2, the metal core of **Au$_{19}$Ag$_6$** is a centered icosahedral Au@Au$_6$Ag$_6$ core, similar to the Au$_{13}$ core in [Au$_{25}$(SR)$_{18}$]$^-$. However, the icosahedron is slightly distorted due to the incorporation of Ag atoms. The Au–Au bond lengths from the central gold atom to the vertices of the Au$_6$Ag$_6$ icosahedron are between 2.7908(15) and 2.8189(14) Å (average 2.806 Å), and the Au–Ag bond lengths from the central gold atom to the silver vertices of the Au$_6$Ag$_6$ icosahedron are between 2.962(2) and 3.085(2) Å (average 3.022 Å). The Au–Au distances in the Au$_6$Ag$_6$ icosahedron can be classified into two groups: the shorter ones average 2.670 Å and the longer ones average 3.289 Å, which are distinguished by whether they interact with V-shaped [Au$_2$(SR)$_3$] staples or not. The Au–Ag bond lengths on the Au$_6$Ag$_6$ shell are in the range of 2.824(2)–3.056(2) Å (average 2.922 Å).

As shown in Fig. 2b, six dopant Ag atoms are located at two opposite triangles of the icosahedron, and the six gold atoms are in the arrangement of chair conformation. Each of the two Ag$_3$ triangles is capped by a μ$_3$ thiolate. In the Ag$_3$ units, Ag atoms are bound by argentophilic interactions with Ag–Ag distances between 3.462(3) and 3.773(3) Å (average 3.623 Å), and the average bond length of the Ag–S bond is 2.469 Å.[57,58] There are 12 peripheral gold atoms attached to this Au$_6$Ag$_6$ shell (Fig. 2c), but the gold-thiolate motifs are different from [Au$_{25}$(SR)$_{18}$]$^-$ due to the coordination of 6 PPh$_3$ (Fig. 2d).
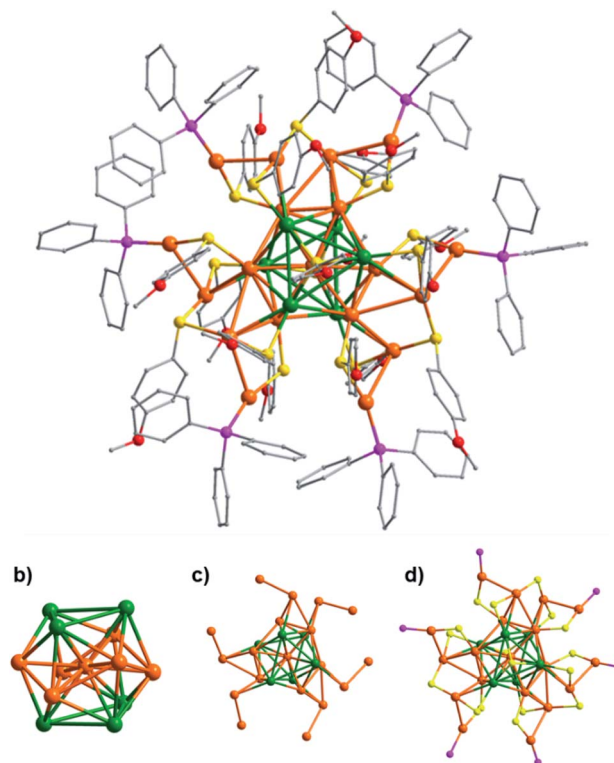

Fig. 2 (a) Molecular structure of **Au$_{19}$Ag$_6$**. Au orange, Ag green, P purple, S yellow, C gray, and O red. (b) The centered icosahedral Au$_7$Ag$_6$ core. (c) Au$_7$Ag$_6$ with the 12 exterior Au atoms. (d) Au$_7$Ag$_6$ with three V-shaped [Au$_2$(SR)$_3$] staples and six [P–Au–SR] staples.

As shown in Fig. 3, **Au$_{19}$Ag$_6$** has three dimeric staples ([Au$_2$(SR)$_3$], motif A) and six semi-staples ([P–Au–SR], motif B), which is quite different from [Au$_{25}$(SR)$_{18}$]$^-$ that has six identical [Au$_2$(SR)$_3$] dimeric staples. In the present case, each [Au$_2$(SR)$_3$] staple is connected to two Ag atoms in the Au$_6$Ag$_6$ shell, while each [P–Au–SR] semi-staple is linked to one Au atom of Au$_6$Ag$_6$.[59] Therefore, the sites for silver and gold in the Au$_6$Ag$_6$

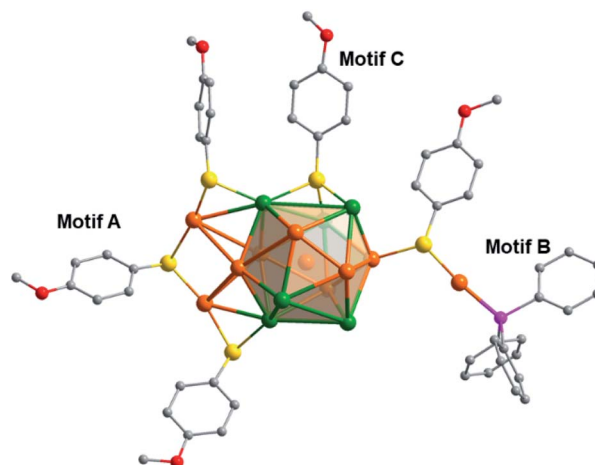**Fig. 3** Gold-thiolate motifs attached to the Au$_6$Ag$_6$ shell (some of the surface binding motifs are removed for clarity).

shell can be differentiated by the peripheral motifs through which they are connected. The doping of silver atoms lowers the symmetry from I_h of the Au_{13} kernel in $[Au_{25}(SR)_{18}]^-$ to D_3 of the Au_7Ag_6 core in the title cluster.

Studies have shown that the difficulty in achieving ordered doping in $Au_{25-x}Ag_x(SR)_{18}$ might be attributed to the highly symmetric geometry of $[Au_{25}(SR)_{18}]^-$. Negishi *et al.* found that Ag substitution tends to occur at specific sites, where the substituted Au atoms are not equivalent to the other Au atoms.[60] As for the title cluster, its synthesis involves two steps, that is, the reduction of the gold precursor and the subsequent addition of silver thiolate. We performed ESI-MS for the reaction mixture before adding silver thiolate, and no peak of $[Au_{25}(SR)_{18}]^-$ or $[Au_{25}(MeOPhS)_{17}(PPh_3)_6]^{2+}$ was observed. Therefore, the formation mechanism is not a simple substitution of gold with silver in Au_{25}, and it may involve the reaction of unknown intermediate clusters with silver thiolate.

We believe that the precise location of Ag atoms in **$Au_{19}Ag_6$** is due to the introduction of the Ph_3P ligand. Because of the stronger bonding of Au–P than Ag–P, the metal atoms that coordinate to the PPh_3 ligands are all Au atoms. In comparison, Ag atoms preferentially take the positions that are bound to the S atoms of thiolates. ^{31}P-NMR of **$Au_{19}Ag_6$** in CD_2Cl_2 has only one peak at 37.48 ppm (Fig. S1†), which confirms that there is only one kind of P in **$Au_{19}Ag_6$** consistent with its D_3 symmetry.

In this dual-ligand system, Au and Ag atoms are fixed at special positions to form precisely substituted gold-silver nanoclusters. Similar situations have been observed in halogen/phosphine co-protected rod-like M_{25} nanoclusters as well as M_{38} alloy nanoclusters.[61–65] For the M_{25} rod-like cluster, because the Ag–Cl bond is stronger than Au–Cl and Au–P is stronger than Ag–P, Ag atoms occupy all the positions bound to chlorides, while Au atoms preferentially take the positions linked to PPh_3. It is worth mentioning that in a system where thiolates and phosphines coexist, it is easy to obtain thiolate/phosphine/chloride co-protected rod-like $Au_{25-x}Ag_x$ nanoclusters, but this problem can be avoided by removing the Cl in PPh_3AuCl during the synthesis process.

The absorption spectrum of **$Au_{19}Ag_6$** is shown in Fig. 4, which exhibits two prominent absorption peaks at 390 nm and 463 nm. In comparison with $Au_{25-x}Ag_x$ with disordered doping, it is found that the UV spectrum of **$Au_{19}Ag_6$** is very different.[24] Remarkably, the prominent peak around 700 nm in

$[Au_{25}(SR)_{18}]^-$ disappears in **$Au_{19}Ag_6$**. Such a difference is generated from the alteration in electronic structures.[66,67] The number of valence electrons of **$Au_{19}Ag_6$** is 6 ($n = 19 + 6 - 17 - 2$), corresponding to the superatomic electronic configuration $1S^21P^4$ in contrast to $1S^21P^6$ of $[Au_{25}(SR)_{18}]^-$.[68,69] Thus, the HOMO–LUMO transition is an optically forbidden p–p transition as confirmed by the following TDDFT calculations, which explains the disappearance of the ~700 nm peak. Notably, the geometry of **$Au_{19}Ag_6$** is oblate as shown in Fig. 2. The Au atoms in the staples are distributed on the waist of the icosahedron. Such a core distortion in **$Au_{19}Ag_6$** is in line with its 6e configuration.[45] Unlike thiol-protected Au_{25} or $Au_{25-x}Ag_x$ clusters, the use of neutral phosphine ligands in **$Au_{19}Ag_6$** makes the system more positively charged,[45,70] leading to the formation of a 6e system instead of 8e. A similar case was observed in $[Au_{40}(PhC\equiv C)_{20}(dppm)_4](SbF_6)_4$ (dppm = bis(diphenylphosphino) methane), where it is a 16e system instead of 18e.[59]

Time-dependent density functional theory (TDDFT) calculations were carried out to explore the relationship between the electronic structure and optical absorption properties. We adopted the structural data from X-ray single crystal diffraction
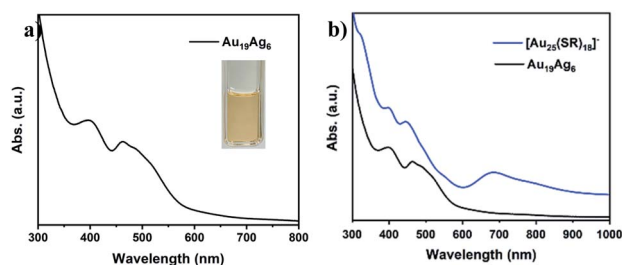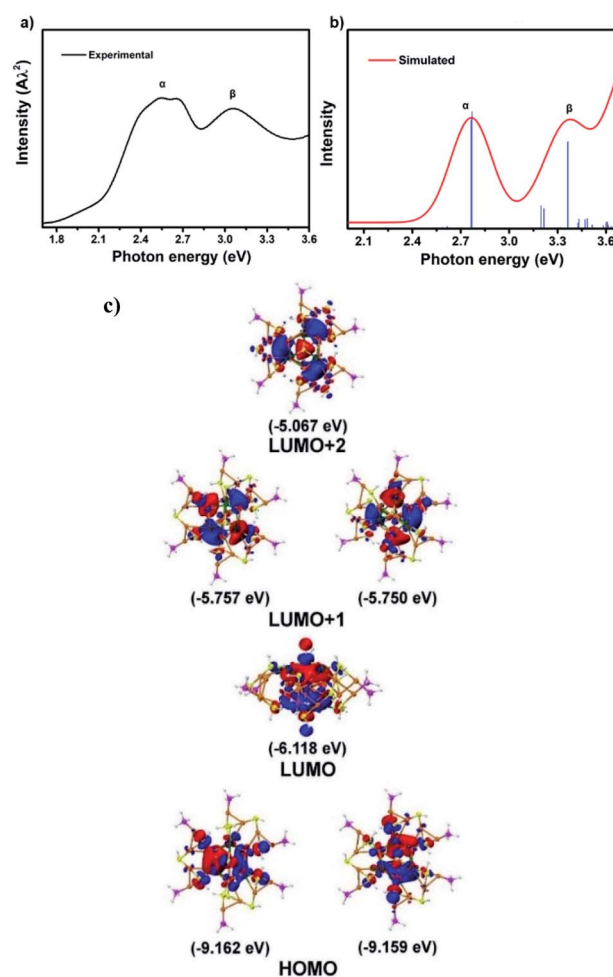

Fig. 5 (a) Experimental absorption spectrum of **$Au_{19}Ag_6$**. (b) Simulated spectrum of **$Au_{19}Ag_6$**. (c) Frontier orbitals including the HOMO, LUMO, LUMO+1 and LUMO+2 of **$Au_{19}Ag_6$**.
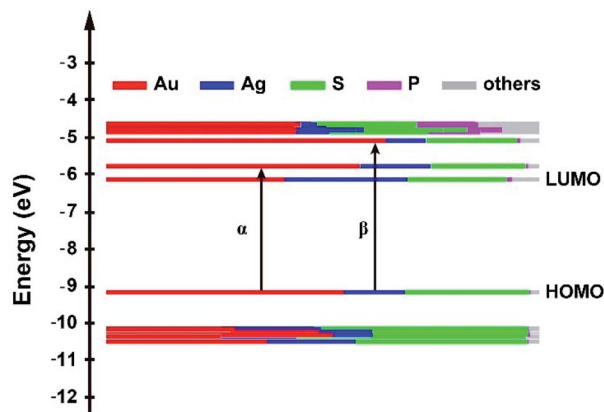

Fig. 4 (a) The absorption spectrum of **$Au_{19}Ag_6$** in CH_2Cl_2. Inset: photograph of the solution. (b) The comparison of **$Au_{19}Ag_6$** and $[Au_{25}(SR)_{18}]^-$.

Fig. 6 Kohn–Sham molecular orbital energy levels of **Au$_{19}$Ag$_6$**.

as an input file to the quantum chemistry program Gaussian 16. As shown in Fig. 5a, there are characteristic absorption peaks at 2.78 eV (α) and 3.38 eV (β) in the simulated spectrum, which fit well with the experimental results except for a slight blue shift (Fig. 6b). The band at 2.78 eV was referred to as the transition from the HOMO to the LUMO+1, whereas the β peak at 3.38 eV was assigned to the HOMO to LUMO+2 transition. It is worth noting that **Au$_{19}$Ag$_6$** exhibits highly symmetric superatomic orbital properties with the HOMO–LUMO showing P orbital characteristics, which accounts for the optically forbidden transition from the HOMO to the LUMO.

According to the Kohn–Sham molecular orbital (MO) energy level diagram of **Au$_{19}$Ag$_6$** (Fig. 6), the HOMO and LUMO+1 orbitals are mainly constituted by the Au and Ag atomic orbitals in the Au$_7$Ag$_6$ icosahedral core. Therefore, the α absorption band at 2 eV and the β peak at 3.38 eV (Fig. 6b) are primarily attributed to the charge transfer within the metal kernel. Notably, the atomic orbitals of P contribute little to KS molecular orbitals.

4. Conclusion

In summary, we have obtained a bimetal nanocluster with ordered silver doping. This cluster has a precise composition and well-defined molecular structure, in which dopant silver atoms are located at the two opposite triangle sites in the distorted icosahedral Au@Au$_6$Ag$_6$ core. This cluster exhibits totally different optical properties from previously reported Au$_{25-x}$Ag$_x$ and Au$_{25}$ clusters, due to its 1S^{2}1P^4 electronic configuration. This is the first example of doping silver atoms in a spherical Au$_{25}$ cluster at specific sites in an ordered way. This work underlies the effectiveness of using a ligand combination strategy to generate alloy nanoclusters with special geometric and electronic structures.

Data availability

The X-ray crystallographic structure reported in this article has been deposited at the Cambridge Crystallographic Data Centre (CCDC) with deposition number (CCDC 2131886).

Author contributions

Q.-M. W. conceived and directed the project. W.-Q. S. performed the experiments. Z.-J. G. conducted the calculations. Z.-J. G., J.-J. L and X.-S. H. analyzed the crystal data. All the authors discussed the results and co-wrote the manuscript.

Conflicts of interest

There are no conflicts to declare.

Acknowledgements

Notes and references

1 Y. Du, H. Sheng, D. Astruc and M. Zhu, *Chem. Rev.*, 2020, **120**, 526–622.

2 Z. Lei, X.-K. Wan, S.-F. Yuan, Z.-J. Guan and Q.-M. Wang, *Acc. Chem. Res.*, 2018, **51**, 2465–2474.

3 Q. Yao, Z. Wu, Z. Liu, Y. Lin, X. Yuan and J. Xie, *Chem. Sci.*, 2021, **12**, 99–127.

4 Z.-J. Guan, F. Hu, J.-J. Li, Z.-R. Liu and Q.-M. Wang, *Nanoscale*, 2020, **12**, 13346–13350.

5 J.-J. Li, Z.-J. Guan, Z. Lei, F. Hu and Q.-M. Wang, *Angew. Chem., Int. Ed.*, 2019, **58**, 1083–1087.

6 P. D. Jadzinsky, G. Calero, C. J. Ackerson, D. A. Bushnell and R. D. Kornberg, *Science*, 2007, **318**, 430–433.

7 S.-F. Yuan, R.-L. He, X.-S. Han, J.-Q. Wang, Z.-J. Guan and Q.-M. Wang, *Angew. Chem., Int. Ed.*, 2021, **60**, 14345–14349.

8 X. Kang, H. Chong and M. Zhu, *Nanoscale*, 2018, **10**, 10758–10834.

9 Z. Gan, N. Xia and Z. Wu, *Acc. Chem. Res.*, 2018, **51**, 2774–2783.

10 W. Li, C. Liu, H. Abroshan, Q. Ge, X. Yang, H. Xu and G. Li, *J. Phys. Chem. C*, 2016, **120**, 10261–10267.

11 C. Yao, J. Chen, M.-B. Li, L. Liu, J. Yang and Z. Wu, *Nano Lett.*, 2015, **15**, 1281–1287.

12 X. Dou, X. Yuan, Q. Yao, Z. Luo, K. Zheng and J. Xie, *Chem. Commun.*, 2014, **50**, 7459–7462.

13 J. Xiang, P. Li, Y. Song, X. Liu, H. Chong, S. Jin, Y. Pei, X. Yuan and M. Zhu, *Nanoscale*, 2015, **7**, 18278–18283.

14 Y. Li, T.-Y. Luo, M. Zhou, Y. Song, N. L. Rosi and R. Jin, *J. Am. Chem. Soc.*, 2018, **140**, 14235–14243.

15 C. Kumara and A. Dass, *Nanoscale*, 2012, **4**, 4084–4086.

16 Z.-J. Guan, J.-L. Zeng, S.-F. Yuan, F. Hu, Y.-M. Lin and Q.-M. Wang, *Angew. Chem., Int. Ed.*, 2018, **57**, 5703–5707.

17 J.-L. Zeng, Z.-J. Guan, Y. Du, Z.-A. Nan, Y.-M. Lin and Q.-M. Wang, *J. Am. Chem. Soc.*, 2016, **138**, 7848–7851.

18 S. Wang, X. Meng, A. Das, T. Li, Y. Song, T. Cao, X. Zhu, M. Zhu and R. Jin, *Angew. Chem., Int. Ed.*, 2014, **53**, 2376–2380.

19 C. M. Aikens, *J. Phys. Chem. C*, 2008, **112**, 19797–19800.

20 K. R. Krishnadas, A. Baksi, A. Ghosh, G. Natarajan and T. Pradeep, *ACS Nano*, 2017, **11**, 6015–6023.

21 M. Zhu, C. M. Aikens, F. J. Hollander, G. C. Schatz and R. Jin, *J. Am. Chem. Soc.*, 2008, **130**, 5883–5885.

22 M. W. Heaven, A. Dass, P. S. White, K. M. Holt and R. W. Murray, *J. Am. Chem. Soc.*, 2008, **130**, 3754–3755.

23 X. Kang, Y. Li, M. Zhu and R. Jin, *Chem. Soc. Rev.*, 2020, **49**, 6443–6514.

24 Y. Negishi, T. Iwai and M. Ide, *Chem. Commun.*, 2010, **46**, 4713–4715.

25 J.-P. Choi, C. A. Fields-Zinna, R. L. Stiles, R. Balasubramanian, A. D. Douglas, M. C. Crowe and R. W. Murray, *J. Phys. Chem. C*, 2010, **114**, 15890–15896.

26 C. Kumara, C. M. Aikens and A. Dass, *J. Phys. Chem. Lett.*, 2014, **5**, 461–466.

27 R. Jin, S. Zhao, C. Liu, M. Zhou, G. Panapitiya, Y. Xing, N. L. Rosi, J. P. Lewis and R. Jin, *Nanoscale*, 2017, **9**, 19183–19190.

28 Q. Li, S. Wang, K. Kirschbaum, K. J. Lambright, A. Das and R. Jin, *Chem. Commun.*, 2016, **52**, 5194–5197.

29 S. Wang, Y. Song, S. Jin, X. Liu, J. Zhang, Y. Pei, X. Meng, M. Chen, P. Li and M. Zhu, *J. Am. Chem. Soc.*, 2015, **137**, 4018–4021.

30 K. R. Krishnadas, A. Ghosh, A. Baksi, I. Chakraborty, G. Natarajan and T. Pradeep, *J. Am. Chem. Soc.*, 2016, **138**, 140–148.

31 K. R. Krishnadas, A. Baksi, A. Ghosh, G. Natarajan and T. Pradeep, *Nat. Commun.*, 2016, **7**, 13447.

32 S. Yamazoe, W. Kurashige, K. Nobusada, Y. Negishi and T. Tsukuda, *J. Phys. Chem. C*, 2014, **118**, 25284–25290.

33 S. Hossain, T. Ono, M. Yoshioka, G. Hu, M. Hosoi, Z. Chen, L. V. Nair, Y. Niihori, W. Kurashige, D.-e. Jiang and Y. Negishi, *J. Phys. Chem. Lett.*, 2018, **9**, 2590–2594.

34 H. Qian, W. T. Eckenhoff, Y. Zhu, T. Pintauer and R. Jin, *J. Am. Chem. Soc.*, 2010, **132**, 8280–8281.

35 S.-F. Yuan, C.-Q. Xu, J. Li and Q.-M. Wang, *Angew. Chem., Int. Ed.*, 2019, **58**, 5906–5909.

36 Z.-J. Guan, J.-L. Zeng, Z.-A. Nan, X.-K. Wan, Y.-M. Lin and Q.-M. Wang, *Sci. Adv.*, 2016, **2**, e1600323.

37 N. Kobayashi, Y. Kamei, Y. Shichibu and K. Konishi, *J. Am. Chem. Soc.*, 2013, **135**, 16078–16081.

38 X.-K. Wan, Z.-W. Lin and Q.-M. Wang, *J. Am. Chem. Soc.*, 2012, **134**, 14750–14752.

39 X.-S. Han, X. Luan, H.-F. Su, J.-J. Li, S.-F. Yuan, Z. Lei, Y. Pei and Q.-M. Wang, *Angew. Chem., Int. Ed.*, 2020, **59**, 2309–2312.

40 W.-D. Liu, J.-Q. Wang, S.-F. Yuan, X. Chen and Q.-M. Wang, *Angew. Chem., Int. Ed.*, 2021, **60**, 11430–11435.

41 J. Chen, Q.-F. Zhang, T. A. Bonaccorso, P. G. Williard and L.-S. Wang, *J. Am. Chem. Soc.*, 2014, **136**, 92–95.

42 F. Hu, J.-J. Li, Z.-J. Guan, S.-F. Yuan and Q.-M. Wang, *Angew. Chem., Int. Ed.*, 2020, **59**, 5312–5315.

43 Y. Chen, C. Zeng, C. Liu, K. Kirschbaum, C. Gayathri, R. R. Gil, N. L. Rosi and R. Jin, *J. Am. Chem. Soc.*, 2015, **137**, 10076–10079.

44 P. R. Nimmala and A. Dass, *J. Am. Chem. Soc.*, 2014, **136**, 17016–17023.

45 Y. Du, Z. J. Guan, Z. R. Wen, Y. M. Lin and Q. M. Wang, *Chem.–Eur. J.*, 2018, **24**, 16029–16035.

46 S. S. Zalesskiy, A. E. Sedykh, A. S. Kashin and V. P. Ananikov, *J. Am. Chem. Soc.*, 2013, **135**, 3550–3559.

47 I. Medina-Mercado, A. Colin-Molina, J. E. Barquera-Lozada, B. Rodríguez-Molina and S. Porcel, *ACS Catal.*, 2021, **11**, 8968–8977.

48 M. J. Frisch, G. W. Trucks, H. B. Schlegel, G. E. Scuseria, M. A. Robb, J. R. Cheeseman, G. Scalmani, V. Barone, G. A. Petersson, H. Nakatsuji, X. Li, M. Caricato, A. V. Marenich, J. Bloino, B. G. Janesko, R. Gomperts, B. Mennucci, H. P. Hratchian, J. V. Ortiz, A. F. Izmaylov, J. L. Sonnenberg, D. Williams-Young, F. Ding, F. Lipparini, F. Egidi, J. Goings, B. Peng, A. Petrone, T. Henderson, D. Ranasinghe, V. G. Zakrzewski, J. Gao, N. Rega, G. Zheng, W. Liang, M. Hada, M. Ehara, K. Toyota, R. Fukuda, J. Hasegawa, M. Ishida, T. Nakajima, Y. Honda, O. Kitao, H. Nakai, T. Vreven, K. Throssell, J. A. Montgomery Jr, J. E. Peralta, F. Ogliaro, M. J. Bearpark, J. J. Heyd, E. N. Brothers, K. N. Kudin, V. N. Staroverov, T. A. Keith, R. Kobayashi, J. Normand, K. Raghavachari, A. P. Rendell, J. C. Burant, S. S. Iyengar, J. Tomasi, M. Cossi, J. M. Millam, M. Klene, C. Adamo, R. Cammi, J. W. Ochterski, R. L. Martin, K. Morokuma, O. Farkas, J. B. Foresman and D. J. Fox, *Gaussian 16, Revision B.01*, Gaussian Inc., Wallingford CT, 2016.

49 P. J. Hay and W. R. Wadt, *J. Chem. Phys.*, 1985, **82**, 299–310.

50 A. D. Becke, *Phys. Rev. A*, 1988, **38**, 3098–3100.

51 D. Coskun, S. V. Jerome and R. A. Friesner, *J. Chem. Theory Comput.*, 2016, **12**, 1121–1128.

52 W. Humphrey, A. Dalke and K. Schulten, *J. Mol. Graphics*, 1996, **14**, 33–38.

53 T. Lu and F. Chen, *J. Comput. Chem.*, 2012, **33**, 580–592.

54 B. K. Teo and H. Zhang, *Angew. Chem., Int. Ed.*, 1992, **31**, 445–447.

55 X.-K. Wan, J.-Q. Wang and Q.-M. Wang, *Angew. Chem., Int. Ed.*, 2021, **60**, 20748–20753.

56 Crystal data for **Au$_{19}$Ag$_6$**: C$_{227}$H$_{209}$Ag$_6$Au$_{19}$B$_2$F$_8$O$_{17}$P$_6$S$_{17}$, triclinic, P-1, a = 20.4536(6) Å, b= 20.7898(7) Å, c = 33.6586(9) Å, α = 72.945(3)°, β = 82.104(2)°, γ = 63.917(3)°, V = 12289.0(8) Å^3, Z = 2, T = 173 K, 77948 reflections measured, 39715 unique (R_{int}= 0.0992), final R_1=0.0853, and wR_2= 0.2442 for 77948 observed reflections [$I > 2\sigma(I)$]. Deposition number 2131886 contains the supplementary crystallographic data for this paper.†

57 H. Schmidbaur and A. Schier, *Angew. Chem., Int. Ed.*, 2015, **54**, 746–784.

58 Q.-M. Wang and T. C. W. Mak, *J. Am. Chem. Soc.*, 2001, **123**, 7594–7600.

59 T. Wang, W.-H. Zhang, S.-F. Yuan, Z.-J. Guan and Q.-M. Wang, *Chem. Commun.*, 2018, **54**, 10367–10370.

60 S. Hossain, Y. Niihori, L. V. Nair, B. Kumar, W. Kurashige and Y. Negishi, *Acc. Chem. Res.*, 2018, **51**, 3114–3124.

61 B. K. Teo and K. Keating, *J. Am. Chem. Soc.*, 1984, **106**, 2224–2226.

62 B. K. Teo, X. Shi and H. Zhang, *J. Am. Chem. Soc.*, 1991, **113**, 4329–4331.

63 B. K. Teo, X. Shi and H. Zhang, *J. Chem. Soc., Chem. Commun.*, 1992, 1195–1196, DOI: 10.1039/C39920001195.

64 B. K. Teo, K. Keating and Y. H. Kao, *J. Am. Chem. Soc.*, 1987, **109**, 3494–3495.

65 B. K. Teo, H. Zhang and X. Shi, *J. Am. Chem. Soc.*, 1990, **112**, 8552–8562.

66 K. Kwak, Q. Tang, M. Kim, D.-e. Jiang and D. Lee, *J. Am. Chem. Soc.*, 2015, **137**, 10833–10840.

67 T. Kawawaki, Y. Imai, D. Suzuki, S. Kato, I. Kobayashi, T. Suzuki, R. Kaneko, S. Hossain and Y. Negishi, *Chem.–Eur. J.*, 2020, **26**, 16150–16193.

68 D. M. P. Mingos, *Dalton Trans.*, 2015, **44**, 6680–6695.

69 M. A. Tofanelli, K. Salorinne, T. W. Ni, S. Malola, B. Newell, B. Phillips, H. Häkkinen and C. J. Ackerson, *Chem. Sci.*, 2016, **7**, 1882–1890.

70 A. Cirri, H. Morales Hernández, C. Kmiotek and C. J. Johnson, *Angew. Chem., Int. Ed.*, 2019, **58**, 13818–13822.